Myosin Va cooperates with PKA RIα to mediate maintenance of the endplate in vivo

Ira V. Röder[a], Kyeong-Rock Choi[a], Markus Reischl[b], Yvonne Petersen[a], Markus E. Diefenbacher[a], Manuela Zaccolo[c], Tullio Pozzan[d,e,1], and Rüdiger Rudolf[a,1]

[a]Institute of Toxicology and Genetics; [b]Institute for Applied Computer Science, Karlsruhe Institute of Technology, Hermann-von-Helmholtz-Platz 1, 76344 Eggenstein-Leopoldshafen, Germany; [c]Neuroscience and Molecular Pharmacology, Faculty of Biomedical and Life Sciences, University of Glasgow, University Avenue, Glasgow G12 8QQ, United Kingdom; [d]Venetian Institute of Molecular Medicine, Via Orus 2, 35129 Padua, Italy; and [e]Department of Biomedical Sciences, University of Padua and National Research Council Institute of Neuroscience, Viale G. Colombo 3, 35121 Padua, Italy.

Contributed by Tullio Pozzan, Venetian Institute of Molecular Medicine, Padua, Italy, December 11, 2009 (sent for review September 18, 2009)

Myosin V motor proteins facilitate recycling of synaptic receptors, including AMPA and acetylcholine receptors, in central and peripheral synapses, respectively. To shed light on the regulation of receptor recycling, we employed in vivo imaging of mouse neuromuscular synapses. We found that myosin Va cooperates with PKA on the postsynapse to maintain size and integrity of the synapse; this cooperation also regulated the lifetime of acetylcholine receptors. Myosin Va and PKA colocalized in subsynaptic enrichments. These accumulations were crucial for synaptic integrity and proper cAMP signaling, and were dependent on AKAP function, myosin Va, and an intact actin cytoskeleton. The neuropeptide and cAMP agonist, calcitonin-gene related peptide, rescued fragmentation of synapses upon denervation. We hypothesize that neuronal ligands trigger local activation of PKA, which in turn controls synaptic integrity and turnover of receptors. To this end, myosin Va mediates correct positioning of PKA in a postsynaptic microdomain, presumably by tethering PKA to the actin cytoskeleton.

cAMP | muscle | neuromuscular junction | microdomain | synaptic plasticity

Recently, myosin V motor proteins were found to be crucial for the plasticity of central and peripheral synapses by facilitating, respectively, the recycling of AMPA (1–3) and acetylcholine receptors (AChRs) (4). The neuromuscular junction (NMJ) is the synapse between motor neurons and skeletal muscle fibers. Even though it is formed during ontogenesis and then maintained over the years (5), half-lives ($t_{1/2}$) of a few days are typical for its protein constituents, such as the AChR (6). The high enrichment of AChRs in the postsynapse is regulated by accurate targeting and turnover of this receptor. Vesicular transport is employed for this purpose, using different routes of exocytosis, endocytosis, and recycling (7–9). We identified myosin Va as the first motor protein involved in AChR trafficking and have found it to facilitate its recycling (4). Down-regulation of myosin Va led to a reduced $t_{1/2}$ of AChRs (4) similar to pathological conditions, such as denervation (6, 10–13) or dystrophy (14). A shortened $t_{1/2}$ of AChRs accompanies morphological changes of the NMJ: while NMJs in mouse muscles are normally elliptic and pretzel-shaped (15), they elongate and fragment under pathological conditions (16, 17).

Previous studies have revealed a major role of cAMP signaling in controlling the $t_{1/2}$ of AChRs (12, 18). cAMP is formed upon activation of G protein-coupled receptors and mediates its effects mainly through protein kinase A (PKA). Notably, stimulation of cAMP synthesis rescued AChR lifetime in denervated (12, 19) and dystrophic muscles (14). Several groups have described antagonistic functions of protein kinase C and PKA on AChR persistence and synaptic strength (18, 20, 21): although activation of protein kinase C destabilizes AChRs, PKA activity protects this receptor from such destabilization (18). In this context, the neuropeptide and cAMP agonist, α-calcitonin gene-related peptide (CGRP), is thought to be a prime regulator of PKA activation (18, 20). CGRP is present in motor nerve terminals and is released in an activity-dependent manner (22). Production of cAMP and activation of PKA are induced upon CGRP receptor binding, leading to short- and long-term effects (22): CGRP leads to AChR phosphorylation (23), increased AChR (20, 24) and decreased acetylcholine esterase expression (25, 26), and NMJ-strength potentiation (27). Thus, CGRP seems to be a trophic factor for the NMJ by local stimulation of cAMP signaling.

The second messenger, cAMP, modulates many cellular functions in response to a variety of stimuli. To assure specificity of the cellular output to different ligands, spatiotemporal compartmentation of the cAMP/PKA pathway into distinct PKA microdomains is thought to be essential (28). Inactive PKA is an heterotetramer consisting of two regulatory (PKA R) and two catalytic subunits, but the catalytic subunits dissociate from the regulatory peptides upon activation by cAMP and phosphorylate target molecules. PKA R exist in four isoforms, RIα/β and RIIα/β. Seemingly, α-isoforms prevail in skeletal muscle (29, 30) and PKA RIα mRNA and protein are enriched in the NMJ region (29–31). PKA microdomain organization is formed through binding of PKA R to A-kinase anchoring proteins (AKAP) (32). Their interaction is the result of a dimerization/docking (DD) domain and an amphipathic α-helix on PKA R and AKAP, respectively. PKA R isoform-specific AKAP disruptor peptides were developed, such as the RI anchoring disruptor (RIAD) peptide for PKA RI (33).

We have recently created cAMP sensors, which were targeted in an AKAP-dependent manner into distinct PKA microdomains, and allowed their functional characterization in heart muscle cells (34) and skeletal muscle fibers in vivo (35). The probes are composed of DD-domains followed by a cAMP sensor based on the "exchange protein directly activated by cAMP" (Epac). Epac-based cAMP sensors bear a cAMP-binding domain of Epac between the GFP mutants CFP and YFP (36). Thus, while CFP or YFP fluorescence of these probes indicate the localization of a PKA microdomain, changes in cAMP levels ([cAMP]) within the microdomain are monitored by alterations in Förster resonance energy transfer (FRET). Here we show a functional link between PKA microdomain organization, myosin Va-based AChR trafficking, and activity-dependent maintenance of the NMJ. Notably, these experiments were carried out in the live, anesthetized mouse after transfection of skeletal muscles.

Results

PKA RIα Is Enriched Below NMJs In Vivo. Formation and localization of PKA RIα dimers in live mouse muscle were investigated by using the bimolecular fluorescence complementation (BiFC)

Author contributions: I.V.R., M.Z., T.P., and R.R. designed research; I.V.R., Y.P., and R.R. performed research; K.-R.C., M.R., and M.E.D. contributed new reagents/analytic tools; I.V.R., M.R., and R.R. analyzed data; and I.V.R., M.Z., T.P., and R.R. wrote the paper.

The authors declare no conflict of interest.

[1]To whom correspondence may be addressed. E-mail: tullio.pozzan@unipd.it or ruediger.rudolf@kit.edu

This article contains supporting information online at www.pnas.org/cgi/content/full/0914087107/DCSupplemental.

approach. In BiFC experiments, nonfluorescent halves of a GFP mutant reconstitute a fluorescent molecule, if both are brought together via dimerizing fusion proteins (37). We generated BiFC constructs containing full-length PKA RIα and N- (VN) or C-terminal halves (VC) of the GFP mutant Venus (Fig. 1*A*). Ten days upon cotransfection of both constructs into tibialis anterior (TA) muscles in live mice, we labeled NMJs with fluorescent α-bungarotoxin (BGT-AF647), a marker of AChRs, and monitored BiFC and BGT fluorescence by in vivo confocal microscopy. Because, under these conditions, transgenic and endogenous PKA RIα might partially interact and, also because homo-dimers of transgenic PKA RIα would be nonfluorescent, it is likely that only a minor portion of PKA RIα was visible by BiFC. Nonetheless, a clear enrichment of BiFC was observed, primarily in puncta below NMJs (Fig. 1*B*; Fig. S1, *Top*). Conversely, coexpression of DD-domain-lacking PKA RIα BiFC constructs (ΔDD-RIα-VN and ΔDD-RIα-VC) with cytoplasmic mCherry did not show such BiFC signals (Fig. S1, *Middle*). Subsynaptic BiFC signals were also not observed upon coexpression of full-length PKA RIα BiFC constructs with AKAP disruptor peptide, RIAD-mCherry (Fig. S1, *Bottom*). These data strongly suggest that PKA RIα dimerizes and accumulates close to NMJs in a DD-domain- and AKAP-dependent manner in vivo.

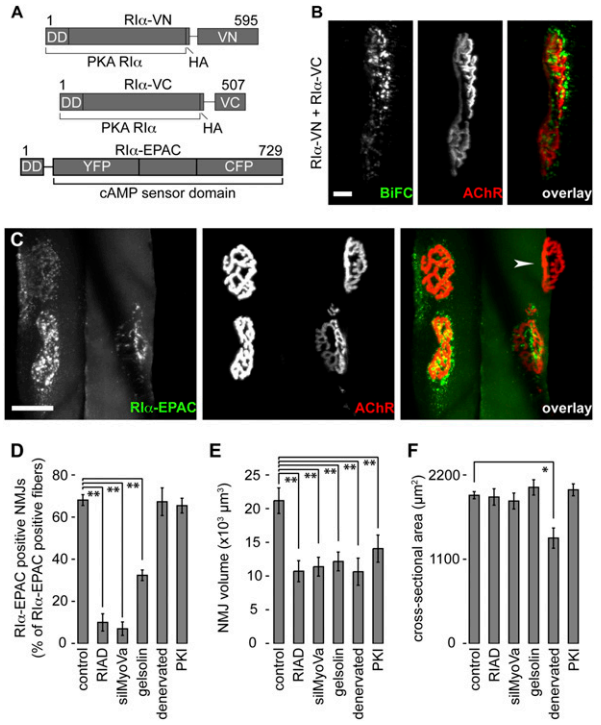

Fig. 1. Subsynaptic accumulation of PKA RIα is only under postsynaptic control; NMJ maintenance also needs presynaptic input. (*A*) Schematic representation of the constructs used for in vivo localization of PKA RIα. The upper two constructs were used in *B*, the lower in *C* to *F*. (*B* and *C*) Representative images show three-dimensional (3D) projections of muscle fibers either expressing PKA RIα-BiFC constructs (*B*) or RIα-EPAC (*C*). Overlays, BiFC, or RIα-EPAC (*green*); AChRs (BGT-AF647) (*red*). [Scale bars, 10 µm (*B*) and 50 µm (*C*).] *Arrowhead* in *C*, NMJ of a fiber not expressing RIα-EPAC. (*D–F*) Graphs showing either the fractions of NMJs exhibiting accumulations of RIα-EPAC (*D*), the NMJ volumes (*E*), or the cross-sectional areas per fiber (*F*) under different experimental conditions. Muscles were either transfected with RIα-EPAC (control and denervated) or cotransfected with RIα-EPAC and RIAD, silMyoVa, gelsolin, or PKI (indicated below bars) and 10 days later imaged with in vivo confocal microscopy. NMJs were labeled with BGT-AF647 shortly before imaging. Cross-sectional areas were determined on transversal slices taken from some muscles. Graphs show mean values of *n* independent experiments ± SEM. *n*-values in *D* and *E*: control, ≥11; RIAD, ≥10; silMyoVa, ≥6; gelsolin, ≥5; denervated, ≥5; PKI ≥6. *n* = 4 in *F*. For all conditions ≥90 NMJs (*D* and *E*) and ≥400 fibers (*F*) were analyzed.

Inhibition of AKAP or Myosin Va Function, but Not of Neuronal Input, Ablates Subsynaptic Enrichment of PKA RIα In Vivo. Next, we investigated if myosin Va and PKA cooperate for the maintenance of NMJ integrity. To this end, we first expressed in live mouse TA muscle EPAC sensors, which are either targeted to the PKA RIα- (RIα-EPAC) (Fig. 1*A*) or the PKA RIIα- (RIIα-EPAC) microdomains. Ten days after transfection, muscles were injected with BGT-AF647 to reveal NMJs and fluorescence was monitored by in vivo confocal microscopy. While RIIα-EPAC showed no enrichment in the NMJ region, RIα-EPAC clearly accumulated below NMJs (Fig. 1*C* shows a 3D projection; *arrowhead*, NMJ of a RIα-EPAC-negative fiber). This result confirmed our BiFC data (Fig. 1*B*). Quantification (see Fig. S2 for the procedure) revealed that ~70% of all fibers expressing RIα-EPAC exhibited subsynaptic clusters of the PKA RIα marker (Fig. 1*D*). Morphologically, both RIα-EPAC-positive and -negative NMJs were quite similar and we could not detect a significant difference in NMJ size between both groups. Coexpression of RIAD strongly reduced RIα-EPAC localization in the NMJ area to ~10% of all RIα-EPAC-expressing fibers (Fig. 1*D* and Fig. S3). Notably, a similar reduction of subsynaptic PKA RIα marker localization was also observed upon coexpression of siRNA against myosin Va (silMyoVa) (Fig. 1*D* and Fig. S3). Furthermore, because myosin Va is dependent on the actin cytoskeleton for proper function (38), we asked whether altering the actin dynamics would exert a comparable effect. We thus coexpressed the actin severing protein, gelsolin-GFP (39), with RIα-EPAC. In addition, this treatment strongly reduced the subsynaptic enrichments of the PKA RIα marker (Fig. 1*D* and Fig. S3). Immunostainings in muscles not transfected with the Epac sensors showed that gelsolin-GFP also displaced endogenous PKA RIα and myosin Va (Fig. S4 *A* and *B*). To test the role of nerve-input and PKA activity, we quantified RIα-EPAC accumulation in denervated muscles and muscles transfected with the protein kinase A-specific inhibitor, PKI (40). These treatments did not affect sensor localization, suggesting that postsynaptic clustering of PKA RIα occurs independently of nerve and PKA activity (Fig. 1*D* and Fig. S3).

NMJ Maintenance Depends on Neuronal Input and Postsynaptic Enrichment of PKA RIα In Vivo. Previously we described that interference with myosin Va function leads to severe size reduction of NMJs (4). Now we have found that the same treatment also delocalized PKA RIα from its subsynaptic site (Fig. 1*D*). To investigate if the ablation of PKA RIα subsynaptic enrichment might itself be a trigger for the size-reducing effect of myosin Va inhibition, we tested whether the block of AKAP function or alteration of the actin cytoskeleton would affect NMJ size as well. Indeed, quantitative analyses (see Fig. S2 for the procedure) revealed that NMJ size was significantly reduced by both treatments (Fig. 1*E*). Notably, the observed reduction in NMJ size was not correlated to decreased fiber cross-sectional areas (Fig. 1*F*), showing that it was not caused by fiber shrinkage. Next, we checked whether nerve or PKA function were needed for this activity and found a strong reduction of NMJ areas upon denervation and upon transfection with PKI (Fig. 1*E*). In the case of denervation, but not in the presence of PKI, muscles also showed a decrease in cross-sectional area (Fig. 1*F*).

Turnover of AChRs Is Dependent on Nerve Input and an Intact Postsynaptic Enrichment of PKA RIα In Vivo. To investigate whether the decrease of NMJ size was linked to reduced AChR persistence and morphological integrity of NMJs, we undertook an in vivo pulse/chase-like experiment using differentially labeled

AChR pools (Fig. 2). Ipsilateral TA muscles were cotransfected with RIα-EPAC and RIAD, silMyoVa, gelsolin-GFP, or PKI. Some ipsilateral legs were transfected with RIα-EPAC and denervated. Contralateral muscles served as controls and were transfected with RIα-EPAC. Simultaneously, all muscles were injected with BGT-AF647 to label AChRs exposed to the cell surface at this time point ("old receptors"). The administered BGT-AF647 was present for marking AChRs only within few hours upon injection (4). Ten days later, muscles were injected with BGT-AF555 to label newly formed synaptic AChRs ("new receptors"). Fluorescence signals of old receptors, new receptors, and synapse morphologies were monitored using confocal in vivo microscopy. Automated image analysis (see Fig. S5) revealed that in contrast to control muscles, NMJs of all treated muscles often showed a fragmented morphology (Fig. 2 *B* and *C*), and a higher new receptor/old receptor ratio (Fig. 2 *B* and *D*). This finding indicated that under these conditions, both NMJ integrity and AChR persistence were affected. Given the apparent involvement of cAMP/PKA-dependent signaling in the maintenance of NMJs and the described functions of the cAMP agonistic neuropeptide CGRP, we tested whether this would have any effect on NMJ integrity or on AChR persistence. We thus repeated some of the pulse/chase-like experiments and now added 25 μL of 20 μM CGRP during transfection. Automated analysis revealed that CGRP was able to block NMJ fragmentation upon denervation, but not in the presence of silMyoVa (Fig. 2 B and C). In addition, we could not observe any effect of CGRP on AChR stability (Fig. 2 *B* and *D*).

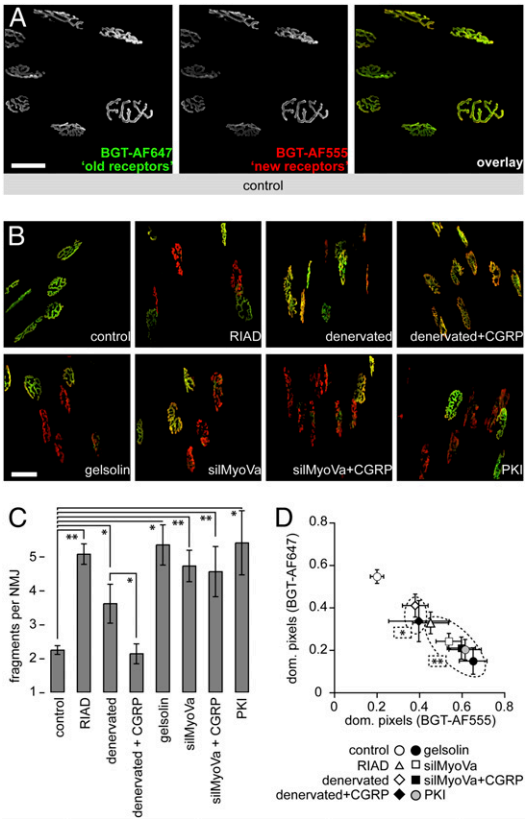

Fig. 2. Persistence of synaptic AChRs and synaptic integrity depend on pre- and postsynaptic factors. TA muscles were transfected with RIα-EPAC (control) or cotransfected with RIα-EPAC and RIAD (RIAD), gelsolin-GFP (gelsolin), PKI (PKI), or silMyoVa (silMyoVa). Some RIα-EPAC-transfected TA muscles were denervated (denervated). During transfection, muscles were coinjected with BGT-AF647 (old receptors) and in some cases also with 25 μL of 20 μM CGRP (+CGRP). Ten days later, muscles were injected with BGT-AF555 (new receptors) and monitored with in vivo confocal microscopy. (Scale bars, 50 μm.) (*A*) Representative 3D projections of old-receptor signals, new-receptor signals and overlay: old receptors (*green*); new receptors (*red*); pixels with similar intensities of both dyes (*yellow*) of a control muscle. (*B*) Representative overlays of all conditions. Colors as in *A*. (*C*) Bar graph, average number of fragments/NMJ from n experiments ± SEM. *n*-values: control, 20 (548 NMJs); RIAD, 4 (57 NMJs); denervated, 7 (246 NMJs); denervated+CGRP, 4 (134 NMJs); gelsolin, 3 (92 NMJs); silMyoVa, 6 (123 NMJs); silMyoVa+CGRP, 6 (199 NMJs); PKI, 6 (190 NMJs). (*D*) Frequency of pixels within each NMJ with dominating old-receptor intensity as a function of pixels where new-receptor signals were prevailing ± SEM. Same data set as in *A*. Significance was tested against control.

CGRP-Induced Rise in [cAMP] in the NMJ Region Is Measureable upon Denervation, but Not upon Block of AKAP or Myosin Va Function in Vivo. Next, we asked whether CGRP-dependent cAMP signaling to PKA RIα might be disturbed by RIAD, inhibition of myosin Va, or denervation. For in vivo monitoring of subsynaptic cAMP signaling, TA muscles were either transfected with RIα-EPAC or cotransfected with RIα-EPAC and RIAD or silMyoVa. Some RIα-EPAC-transfected muscles were denervated. Ten days later, NMJs were marked with BGT-AF647 and FRET-based cAMP measurements were made using in vivo two-photon microscopy (see Fig. S6 for the procedure and probe activity controls). Fibers were illuminated at 810 nm to selectively excite CFP. Emission signals of CFP and YFP were simultaneously recorded. The ratio between the fluorescence intensities emitted from the two chromophores can be conveniently used to dynamically monitor the level of FRET and thus [cAMP] (36, 41). In control muscles, the NMJ localization was easily determined by the accumulated RIα-EPAC fluorescence signals. Upon selecting these regions, most NMJs showed a clear increase in CFP/YFP ratio of the RIα-EPAC probe upon CGRP application (compare Fig. 3 *A* and *C*). Using this probe, only CGRP, but not norepinephrine (NE) was able to raise [cAMP] significantly (Fig. 3*E*). As expected, NE caused a large increase in [cAMP] in fibers transfected with RIIα-EPAC (35). Next, we examined CGRP-induced changes in [cAMP] upon cotransfection with RIAD or silMyoVa. Under these conditions, much less NMJ regions could be identified in the two-photon images, because the accumulation of RIα-EPAC was largely absent. In some cases, however, a slight enrichment was still present, which could be correlated with the localization of BGT-signals in the single photon images. Thus, we selected these regions to determine the subsynaptic changes in [cAMP]. Notably, CGRP did not evoke any measurable change in [cAMP] in the presence of RIAD or silMyoVa (Fig. 3*E*). Conversely, upon denervation we observed a CGRP-dependent rise in [cAMP] similar to that monitored under control conditions (Fig. 3*E*).

PKA RIα Codistributes with Myosin Va and AChRs in Vivo. We then asked whether PKA RIα and myosin Va are localized in the same subsynaptic compartment. To approach this issue, we first used immunostaining and found, that both proteins were highly accumulated next to the synaptic AChR staining (Fig. 4 *A* and *B*) and exhibited small punctate signals at close distance to the NMJ (*arrowheads*, Fig. 4*A3* and *B3*). Next, we wanted to verify, if endogenous PKA RIα and myosin Va colocalized with RIα-EPAC. We thus transfected muscles with our probe and then stained transversal sections of these muscles against AChRs, myosin Va, and a C-terminal epitope of PKA RIα. This revealed a high degree of colocalization between RIα-EPAC and PKA RIα (Fig. 4*C*) or myosin Va (Fig. 4*D*) in the vicinity of the NMJ. To study the codistribution of PKA RIα and myosin Va in vivo, we cotransfected TA muscles with the marker proteins RIα-EPAC and a cargo binding fragment of myosin Va fused to DsRed (MCST-DsRed). The latter has previously been described to be efficiently targeted to the site of endogenous myosin Va (38). We have also recently found that it mimics the distribution of endogenous myosin Va in skeletal muscle and that it does not significantly impair NMJ morphology (4). BGT-AF647 was

CELL BIOLOGY

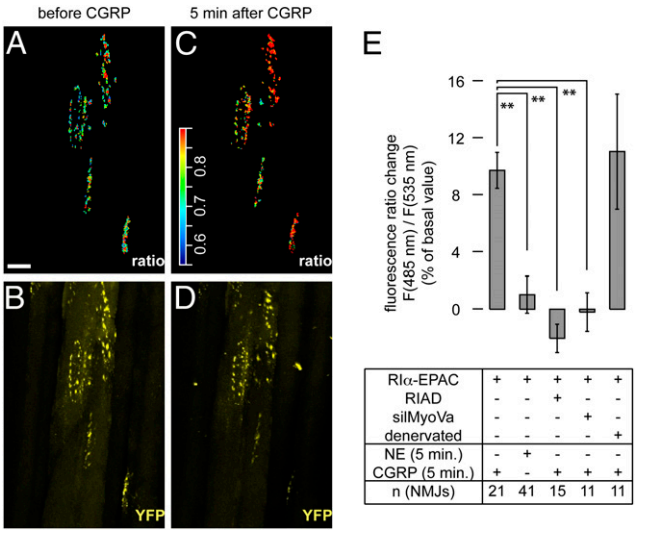

Fig. 3. In the presence of exogenous CGRP, rise in subsynaptic [cAMP] is measurable upon denervation, but not upon impairment of AKAP or myosin Va function. TA muscles were transfected with RIα-EPAC or cotransfected with RIα-EPAC and RIAD (RIAD) or silMyoVa (silMyoVa). Some muscles were transfected with RIα-EPAC and denervated (denervated). Ten days later, muscles were injected with BGT-AF647 and monitored with in vivo two-photon or confocal microscopy. (*A–D*) Representative experiment with a RIα-EPAC-transfected muscle. Images depict 3D projections of the same NMJs before (*A* and *B*) and 5 min after injection of 50 μL of 10 μM CGRP (*C* and *D*). (*A* and *C*) Subsynaptic RIα-EPAC CFP/YFP ratio signals in pseudocolors. (Scale bar, 50 μm.) Color scale bar, pseudocolors corresponding to CFP/YFP ratio values. (*B* and *D*) YFP signals (*yellow*). (*E*) Quantification of different experiments. Shown is the percentage change in CFP/YFP ratio values [*F*(485nm)/*F*(535nm)] compared to basal values upon application of 50 μL of either 10 μM NE or 10 μM CGRP (indicated) ± SEM. Muscles were transfected or denervated as indicated. *n*-values indicated, ≥ three mice per condition.

injected to stain NMJs. In vivo confocal microscopy showed a high degree of overlap between the markers for myosin Va and PKA RIα in close vicinity to NMJs (Fig. 4*E*). In some cases, enrichments of myosin Va- and PKA RIα-positive puncta extended beyond the overlaying NMJ (e.g., lower NMJ in Fig. 4*E*), probably demarcating the disposition of subsynaptic nuclei, which specialize in the expression of NMJ-specific proteins, such as AChRs.

Finally, we investigated if myosin Va and PKA RIα colocalize with endocytosed/recycling AChRs. To this end, we made use of the cell-impermeable BGT-AF647, which marks only surface-exposed or endocytosed/recycling AChRs if applied in vivo. While AChRs are highly concentrated within the postsynaptic membrane, the amount of endocytosed/recycling AChRs is much lower (7). Thus, in Fig. 4*E* there seemed to be no colocalization of myosin Va- and PKA RIα-positive objects with AChR-positive puncta. To detect the low-signal, AChR-positive endocytic/recycling objects, we had to adjust laser and detector gains. Taking care of avoiding signal cross-talk, we took in vivo confocal images to visualize AChR-positive subsynaptic puncta (Fig. 4*F*). This revealed some triple-positive structures. Furthermore, we observed a few double-positive puncta for AChR and either myosin Va or PKA RIα. Quantification yielded ~90% of PKA RIα and myosin Va marker double-positive objects (Fig. 4*G*). Of these, ~30% also contained endocytosed/recycling AChRs (Fig. 4*G*). Similar values were obtained upon quantification of MCST-DsRed-positive puncta. To further substantiate the presence of myosin Va and PKA RIα in a compartment containing endocytosed/recycling AChRs, we performed pull-down experiments of surface-exposed AChRs upon injection of BGT-biotin in the live mouse. This showed coprecipitation of myosin Va and PKA RIα with AChRs. Conversely, PKA RIIα and PKA RIIβ were not coprecipitated (Fig. S7).

Discussion

Myosin V motor proteins have recently been identified as key players in the recycling of postsynaptic receptors. For AMPA receptors, either myosin Va (2) or myosin Vb (1, 3) may be important. We have found myosin Va to be crucial for the maintenance of the neuromuscular synapse, apparently by facilitating recycling of AChRs (4). In extension to this concept, we now present in vivo data showing that for this function, the cooperation of myosin Va with PKA RIα is necessary. Furthermore, we provide strong in vivo evidence that presynaptic cAMP agonists, such as CGRP, are instrumental in activating postsynaptic myosin Va- and PKA RIα-dependent processes and in maintaining the structural integrity of the synapse. We also show that a proper actin cytoskeleton is crucial to efficiently link

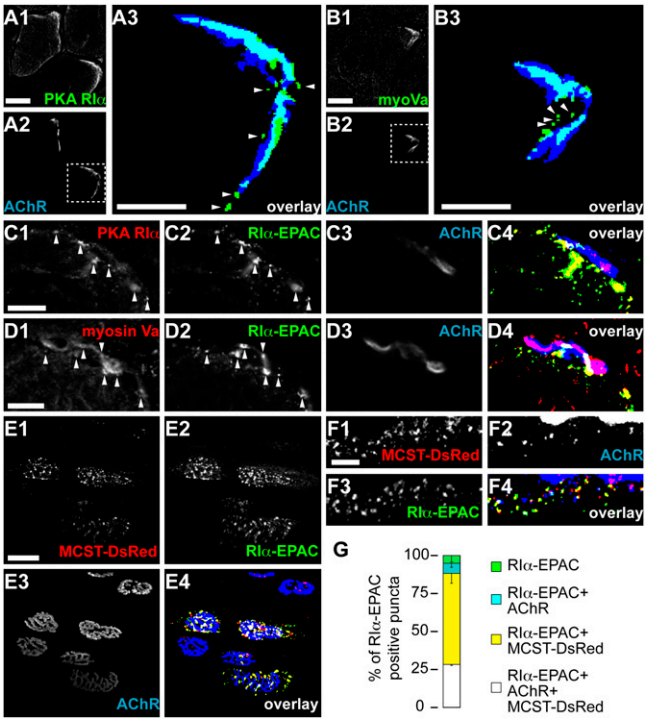

Fig. 4. Myosin Va and PKA RIα share the same subsynaptic compartment. (*A–D*) TA muscles were snap-frozen, sectioned transversally, and immunostained against a C-terminal epitope of PKA RIα or myosin Va. AChRs were labeled with BGT-AF647. Confocal sections depict representative fluorescence signals as indicated. [Scale bars, 50 μm (*A1* to *A2*, *B1* to *B2*) or 10 μm (*A3*, *B3*, *C*, *D*).] (*A3* and *B3*) Overlays, details showing the boxed regions in *A2* and *B2*: immunostaining (*green*), AChR (*blue*). Fluorescence signals, binarized. (*arrowheads*) Punctate PKA RIα- or myosin Va-positive structures. (*C* and *D*) TA muscles were transfected with RIα-EPAC 10 days before staining. (*arrowheads*) RIα-EPAC-positive puncta double-positive for either PKA RIα (*C*) or myosin Va (*D*). Overlays, Fluorescence signals, binarized. PKA RIα/myosin Va (*red*), RIα-EPAC (*green*), AChR (*blue*). Double-positive structures: PKA RIα/myosin Va and RIα-EPAC (*yellow*); PKA RIα/myosin Va and AChR (*magenta*); triple-positive structures (*white*). (*E–G*) TA muscles were cotransfected with MCST-DsRed and RIα-EPAC. Ten days later they were injected with BGT-AF647 and monitored with confocal in vivo microscopy. (*E1–E3*) Representative 3D projections of fluorescence signals of markers as indicated. (Scale bar, 50 μm.) (*F1–F3*) Representative detail of a single optical section. Fluorescence signals of markers as indicated. (Scale bar, 10 μm.) (*E4* and *F4*) Overlays of *E1* to *E3* and *F1* to *F3*, respectively. Fluorescence signals, binarized. MCST-DsRed (*red*), RIα-EPAC (*green*), AChR (*blue*). MCST-DsRed colocalizing with RIα-EPAC (*yellow*). MCST-DsRed colocalizing with AChR (*cyan*). Triple-positive objects (*white*). (*G*) Quantification, fraction of RIα-EPAC-positive puncta also positive for AChR and MCST-DsRed (*white*), MCST-DsRed (*yellow*), AChR (*cyan*), or single positive (*green*). Mean ± SEM (*n* = 3 mice, 2,791 puncta analyzed).

myosin Va and PKA RIα in close proximity to the postsynaptic membrane. This finding might be important for the correct sensing of local, neuronal agonist-induced cAMP signals.

First, using in vivo BiFC and targeted cAMP sensors (Fig. 1), as well as immunostainings (Fig. 4 and Fig. S4), we show that PKA RIα is highly enriched in an AKAP-dependent manner close to the NMJ. To our knowledge, we are unique in providing a demonstration of BiFC in a live, intact mammal. Our PKA localization data confirm similar observations previously made with other approaches (29–31). At present, it is unclear, why under control conditions only about 70% (and not all) RIα-EPAC-positive fibers exhibited accumulations of the probe close to the NMJ. Plausible explanations would be: (*i*) The mRNA of the transgene is not localized as the endogenous one (31), (*ii*) problems in the assignment of NMJs to a specific fiber, and (*iii*) limited amount of binding sites. Notably, subsynaptic localization of our PKA RIα markers was ablated by disrupting the AKAP-PKA RIα interaction, by interfering with myosin Va or by altering the actin cytoskeleton with gelsolin. Furthermore, because all these treatments led to strong decreases in NMJ sizes, this strongly suggests the existence of a functional link between the subsynaptic enrichment of PKA RIα and synaptic integrity. The shrinkage of NMJs did not correlate with fiber cross-sectional area and was therefore a NMJ-specific process. We also noted a strong reduction of NMJ size upon muscle denervation, as previously observed (16, 17, 42), as well as in the presence of PKI; however, these treatments did not disturb subsynaptic accumulation of PKA RIα. Even though denervation resulted in a decreased muscle cross-sectional area, this was not the case with PKI. Although it cannot be excluded that the reductions in NMJ size upon denervation were at least partially caused by a reduced fiber size (43, 44), these data suggest that nerve-derived signals trigger postsynaptic PKA-dependent processes leading to the maintenance of the NMJ size.

To better understand the cellular processes leading to smaller synapses, we further characterized the NMJ integrity and persistence of AChRs upon blocking PKA, AKAP, and myosin Va function, altering the actin cytoskeleton or upon denervation. Whereas AChRs were quite stable under control conditions, all other treatments led to a significantly reduced NMJ integrity and AChR persistence (Fig. 2). While the reduced lifetime of AChRs in the denervated muscles was anticipated from other studies (6, 7, 10, 11), it showed remarkable similarity to the effects of interference with the actin cytoskeleton, PKA anchoring, myosin Va, and PKA function. Notably, injection of a single dose of CGRP blocked NMJ fragmentation upon denervation but not upon transfection with silMyoVa (Fig. 2). We were surprised that a single application of CGRP exerted such a long-lasting effect, and future investigations will address this issue in detail. A simple explanation for this observation is that the local concentration of injected CGRP remains elevated for relatively long time periods (e.g., hours or days). However, this result suggests that myosin Va-driven subsynaptic enrichment of PKA RIα needs nerve-derived signals to maintain NMJ integrity and that CGRP might be one of these. Conversely, CGRP was ineffective with respect to AChR turnover under both conditions. Thus, while the increased NMJ fragmentation and AChR turnover occurring upon inhibition of PKA function indicate that both processes depend on cAMP/PKA signaling, the CGRP rescue data suggest that these two processes are regulated in somewhat different ways. We speculate that, at variance from the NMJ structure maintenance, the regulation of AChR turnover may require activation of another cAMP producing receptor or may be mediated by different mechanisms (e.g., protein modification vs. transcription) that in turn may require different cAMP kinetics/levels.

To test if a particular, subsynaptic cAMP signaling might be relevant in this context, we performed in vivo cAMP monitoring. We found that a CGRP-induced rise in subsynaptic [cAMP] was measureable upon denervation, but not upon block of AKAP or myosin Va function (Fig. 3). To verify that the RIα-EPAC cAMP sensor used could capture PKA RIα-specific changes in [cAMP], we first separately applied the cAMP agonists NE and CGRP. In a recent study performed in the sarcomeric region of muscle fibers in vivo, we showed NE-elicited increments in [cAMP] within a PKA RIIα- but not a PKA RIα-specific microdomain (35). On the contrary, CGRP appeared to stimulate only PKA RIα-specific cAMP responses (35). Now focusing on the subsynaptic region, NE did not evoke any measurable change in the RIα-EPAC signals, while CGRP led to a significant increase in [cAMP] within the PKA RIα-microdomain (Fig. 3). These data corroborate the presence of a PKA RIα-microdomain close to the NMJ, which is sensitive to neuronal agonists like CGRP. We then investigated the cAMP responses in the presence of RIAD and silMyoVa. In both cases, CGRP-induced rises in subsynaptic [cAMP] could not be detected with the RIα-EPAC probe. This could either mean that no cAMP was produced or that the probe, although still in the proximity of the NMJ, was in fact too distant to measure it. The present data do not allow us to distinguish between these two possibilities, and we are trying to develop a methodology to answer this question. Conversely, denervated muscles showed clear rises of [cAMP] upon application of exogenous CGRP indicating that the putative PKA RIα-microdomain was still in place and functional under this condition. These data suggest a cooperative function of myosin Va and PKA RIα for the maintenance of the NMJ. As such, we expected these molecules to be present in the same subsynaptic compartment. Our immunostaining, in vivo imaging and biochemical pull-down data support this hypothesis (Fig. 4, Figs. S4 and S7, and Movie S1).

In conclusion, we provide strong in vivo evidence for a crucial cooperation of myosin Va and PKA RIα in the maintenance of the NMJ. The present results are consistent with the following model. Under normal conditions, AChRs undergo recycling close to the postsynaptic membrane. To this end, they use carriers bearing also myosin Va and PKA RIα. As described for other cell types, such as melanocytes (38) and neuroendocrine cells (45), myosin Va may mediate its function in muscle through a "capture" mechanism: by capturing AChR recycling carriers in the cortical actin, myosin Va prevents carrier dispersal in the large volume of the muscle fiber. PKA RIα, instead, could be necessary to mediate phosphorylation of effector molecules, which are needed for proper delivery of the AChRs to the plasma membrane. Therefore, PKA RIα needs to sense local, nerve-induced cAMP signals in a subsynaptic microdomain. This is achieved by myosin Va-dependent capturing of recycling carriers in the subsynaptic actin cortex.

Materials and Methods

Animals, Transfection, and Denervation. C57BL/6J and C57BL/10J mice were used. Animals were from Charles River and maintained in the local animal facility. Use and care of animals was approved by German authorities and according to national law (TierSchG §§7). Intraperitonial injection of Rompun (Bayer) and Zoletil 100 (Laboratoires Virbac) was used for anesthesia. Transfection was as described (41, 46). For Fig. 2, 25 pmol of BGT-AF647 were coinjected with transfected cDNA. For denervation, 5 mm of the sciatic nerve were removed. Denervation was controlled in killed animals.

Microscopy. All images were made with a DMRE TCS SP2 confocal microscope equipped with a KrAr (488 nm, 514 nm), a diode-pumped (561 nm), a HeNe (633 nm), a Maitai laser (Spectraphysics), a 63×/1.4NA PL APO OIL objective (fixed samples), a 20×/0.7NA HC PL APO CS IMM/CORR UV and a 63×/1.2NA HCX PL APO CS W CORR objective (all Leica Microsystems) (in vivo observation). In vivo immersion medium was Visc-Ophthal gel (Winzer-Pharma). For further experimental details regarding in vivo confocal microscopy see Figs. S1 to S3; for two-photon microscopy, see Fig. S6; for injection of agonists, see Fig. S6; and for confocal microscopy of slices, see Fig. S4.

Muscle Slices. See Fig. S4 for protocol of immunostaining. For determination of cross-sectional areas, sections were moistened with PBS and permeabilized with 0.1% Triton X-100. After washing with PBS, slices were

blocked with 10% FBS/PBS and then incubated with 5-μg/mL wheat germ agglutinin-AF488 (Invitrogen) in 10% FBS/PBS.

Data Analysis. Image analysis employed ImageJ program. For further details regarding the analysis of NMJ size and RIα-EPAC localization in vivo, see Fig. S2; regarding the analysis of old-receptor and new-receptor signal densities and fragmentation, see Fig. S5; for the data analysis of ratiometric videos, see Fig. S6. Regarding the analysis of carrier colocalization in vivo, 3D image stacks were background-subtracted and median filtered. MCST-DsRed or RIα-EPAC signals were binarized and screened for objects of 4 to 20 pxl^2. Object outlines were used as masks in corresponding BGT-AF647, RIα-EPAC or MCST-DsRed images. Objects in masks above background were counted as colocalizing.

Statistics and Graphics. Data were handled using Microsoft Excel. All data shown in graphs represent mean ± SEM, unless otherwise stated. Normal distribution of data sets was tested with the Lilliefors method ($\alpha \leq 0.05$). Variance analysis employed F-test. Significance was tested using Welch test. Significance levels were indicated in figures (*, $P \leq 0.05$; **, $P \leq 0.01$). For data compilation, Adobe Photoshop and Adobe Illustrator were employed.

ACKNOWLEDGMENTS. We thank Drs. Cesetti and Magalhães for critical reading of the manuscript. This study was supported in part by Deutsche Forschungsgemeinschaft Grant RU923/3-1 (to R.R.), Association Francaise contre les Myopathies Grant 12056/13134 (to R.R. and M.Z.), and by a Strategic Project of the University of Padova (T.P.).

1. Lisé MF, et al. (2006) Involvement of myosin Vb in glutamate receptor trafficking. *J Biol Chem* 281:3669–3678.
2. Correia SS, et al. (2008) Motor protein-dependent transport of AMPA receptors into spines during long-term potentiation. *Nat Neurosci* 11:457–466.
3. Wang Z, et al. (2008) Myosin Vb mobilizes recycling endosomes and AMPA receptors for postsynaptic plasticity. *Cell* 135:535–548.
4. Röder IV, et al. (2008) Role of Myosin Va in the plasticity of the vertebrate neuromuscular junction in vivo. *PLoS One* 3:e3871.
5. Lichtman JW, Magrassi L, Purves D (1987) Visualization of neuromuscular junctions over periods of several months in living mice. *J Neurosci* 7:1215–1222.
6. Levitt TA, Salpeter MM (1981) Denervated endplates have a dual population of junctional acetylcholine receptors. *Nature* 291:239–241.
7. Akaaboune M, Culican SM, Turney SG, Lichtman JW (1999) Rapid and reversible effects of activity on acetylcholine receptor density at the neuromuscular junction in vivo. *Science* 286:503–507.
8. Bruneau E, Sutter D, Hume RI, Akaaboune M (2005) Identification of nicotinic acetylcholine receptor recycling and its role in maintaining receptor density at the neuromuscular junction in vivo. *J Neurosci* 25:9949–9959.
9. Bruneau EG, Akaaboune M (2006) The dynamics of recycled acetylcholine receptors at the neuromuscular junction in vivo. *Development* 133:4485–4493.
10. Rotzler S, Schramek H, Brenner HR (1991) Metabolic stabilization of endplate acetylcholine receptors regulated by Ca^{2+} influx associated with muscle activity. *Nature* 349:337–339.
11. Rotzler S, Brenner HR (1990) Metabolic stabilization of acetylcholine receptors in vertebrate neuromuscular junction by muscle activity. *J Cell Biol* 111:655–661.
12. Shyng SL, Xu R, Salpeter MM (1991) Cyclic AMP stabilizes the degradation of original junctional acetylcholine receptors in denervated muscle. *Neuron* 6:469–475.
13. Andreose JS, Xu R, Lømo T, Salpeter MM, Fumagalli G (1993) Degradation of two AChR populations at rat neuromuscular junctions: regulation in vivo by electrical stimulation. *J Neurosci* 13:3433–3438.
14. Xu R, Salpeter MM (1997) Acetylcholine receptors in innervated muscles of dystrophic mdx mice degrade as after denervation. *J Neurosci* 17:8194–8200.
15. Marques MJ, Conchello JA, Lichtman JW (2000) From plaque to pretzel: fold formation and acetylcholine receptor loss at the developing neuromuscular junction. *J Neurosci* 20:3663–3675.
16. Labovitz SS, Robbins N, Fahim MA (1984) Endplate topography of denervated and disused rat neuromuscular junctions: comparison by scanning and light microscopy. *Neuroscience* 11:963–971.
17. Wilson MH, Deschenes MR (2005) The neuromuscular junction: anatomical features and adaptations to various forms of increased, or decreased neuromuscular activity. *Int J Neurosci* 115:803–828.
18. Li MX, Jia M, Jiang H, Dunlap V, Nelson PG (2001) Opposing actions of protein kinase A and C mediate Hebbian synaptic plasticity. *Nat Neurosci* 4:871–872.
19. Caroni P, Rotzler S, Britt JC, Brenner HR (1993) Calcium influx and protein phosphorylation mediate the metabolic stabilization of synaptic acetylcholine receptors in muscle. *J Neurosci* 13:1315–1325.
20. Fontaine B, Klarsfeld A, Changeux JP (1987) Calcitonin gene-related peptide and muscle activity regulate acetylcholine receptor alpha-subunit mRNA levels by distinct intracellular pathways. *J Cell Biol* 105:1337–1342.
21. Lanuza MA, et al. (2006) Phosphorylation of the nicotinic acetylcholine receptor in myotube-cholinergic neuron cocultures. *J Neurosci Res* 83:1407–1414.
22. Poyner DR (1992) Calcitonin gene-related peptide: multiple actions, multiple receptors. *Pharmacol Ther* 56 (1):23–51.
23. Miles K, Greengard P, Huganir RL (1989) Calcitonin gene-related peptide regulates phosphorylation of the nicotinic acetylcholine receptor in rat myotubes. *Neuron* 2: 1517–1524.
24. New HV, Mudge AW (1986) Calcitonin gene-related peptide regulates muscle acetylcholine receptor synthesis. *Nature* 323:809–811.
25. Boudreau-Larivière C, Jasmin BJ (1999) Calcitonin gene-related peptide decreases expression of acetylcholinesterase in mammalian myotubes. *FEBS Lett* 444 (1):22–26.
26. Rossi SG, Dickerson IM, Rotundo RL (2003) Localization of the calcitonin gene-related peptide receptor complex at the vertebrate neuromuscular junction and its role in regulating acetylcholinesterase expression. *J Biol Chem* 278:24994–25000.
27. Lu B, Fu WM, Greengard P, Poo MM (1993) Calcitonin gene-related peptide potentiates synaptic responses at developing neuromuscular junction. *Nature* 363: 76–79.
28. Zaccolo M, et al. (2006) Restricted diffusion of a freely diffusible second messenger: mechanisms underlying compartmentalized cAMP signalling. *Biochem Soc Trans* 34: 495–497.
29. Imaizumi-Scherrer T, Faust DM, Bénichou JC, Hellio R, Weiss MC (1996) Accumulation in fetal muscle and localization to the neuromuscular junction of cAMP-dependent protein kinase A regulatory and catalytic subunits RI alpha and C alpha. *J Cell Biol* 134: 1241–1254.
30. Perkins GA, et al. (2001) PKA, PKC, and AKAP localization in and around the neuromuscular junction. *BMC Neurosci* 2:17.
31. Barradeau S, Imaizumi-Scherrer T, Weiss MC, Faust DM (2001) Muscle-regulated expression and determinants for neuromuscular junctional localization of the mouse RIalpha regulatory subunit of cAMP-dependent protein kinase. *Proc Natl Acad Sci USA* 98:5037–5042.
32. Wong W, Scott JD (2004) AKAP signalling complexes: focal points in space and time. *Nat Rev Mol Cell Biol* 5:959–970.
33. Carlson CR, et al. (2006) Delineation of type I protein kinase A-selective signaling events using an RI anchoring disruptor. *J Biol Chem* 281:21535–21545.
34. Di Benedetto G, et al. (2008) Protein kinase A type I and type II define distinct intracellular signaling compartments. *Circ Res* 103:836–844.
35. Röder IV, et al. (2009) PKA microdomain organisation and cAMP handling in healthy and dystrophic muscle in vivo. *Cell Signal* 21:819–826.
36. Nikolaev VO, Bünemann M, Hein L, Hannawacker A, Lohse MJ (2004) Novel single chain cAMP sensors for receptor-induced signal propagation. *J Biol Chem* 279: 37215–37218.
37. Hu CD, Chinenov Y, Kerppola TK (2002) Visualization of interactions among bZIP and Rel family proteins in living cells using bimolecular fluorescence complementation. *Mol Cell* 9:789–798.
38. Wu X, Bowers B, Rao K, Wei Q, Hammer JA, 3rd (1998) Visualization of melanosome dynamics within wild-type and dilute melanocytes suggests a paradigm for myosin V function in vivo. *J Cell Biol* 143:1899–1918.
39. De Corte V, et al. (2002) Gelsolin-induced epithelial cell invasion is dependent on Ras-Rac signaling. *EMBO J* 21:6781–6790.
40. Day RN, Walder JA, Maurer RA (1989) A protein kinase inhibitor gene reduces both basal and multihormone-stimulated prolactin gene transcription. *J Biol Chem* 264: 431–436.
41. Rudolf R, Magalhães PJ, Pozzan T (2006) Direct in vivo monitoring of sarcoplasmic reticulum Ca^{2+} and cytosolic cAMP dynamics in mouse skeletal muscle. *J Cell Biol* 173: 187–193.
42. Brown MC, Ironton R (1977) Motor neurone sprouting induced by prolonged tetrodotoxin block of nerve action potentials. *Nature* 265:459–461.
43. Coers C, Woolf AL (1959) *The Innervation of Muscle: A Biopsy Study* (Blackwell Scientific Publications, Oxford).
44. Balice-Gordon RJ, Breedlove SM, Bernstein S, Lichtman JW (1990) Neuromuscular junctions shrink and expand as muscle fiber size is manipulated: in vivo observations in the androgen-sensitive bulbocavernosus muscle of mice. *J Neurosci* 10:2660–2671.
45. Rudolf R, et al. (2003) Myosin Va facilitates the distribution of secretory granules in the F-actin rich cortex of PC12 cells. *J Cell Sci* 116:1339–1348.
46. Donà M, et al. (2003) Functional in vivo gene transfer into the myofibers of adult skeletal muscle. *Biochem Biophys Res Commun* 312:1132–1138.